Optics Letters

Femtosecond laser microprinting of a polymer fiber Bragg grating for high-sensitivity temperature measurements

CHI LI, CHANGRUI LIAO,* JIA WANG, ZHENGYONG LI, YING WANG, JUN HE, ZHIYONG BAI, AND YIPING WANG

Key Laboratory of Optoelectronic Devices and Systems of Ministry of Education and Guangdong Province, College of Optoelectronic Engineering, Shenzhen University, Shenzhen 518060, China

**Corresponding author: cliao@szu.edu.cn*

Received 27 May 2018; accepted 18 June 2018; posted 22 June 2018 (Doc. ID 332704); published 12 July 2018

We demonstrate the microprinting of a novel suspended polymer fiber Bragg grating for high-sensitivity temperature measurements. The proposed sensor was developed using a femtosecond laser-induced multiphoton polymerization technique. The grating was cured in a single-groove silica tube spliced between two single-mode fibers. Its transmission spectrum, mode field, and temperature response were thoroughly investigated. A sensitivity of −220 pm/°C was achieved over a temperature range of 24°C to 40°C, which is meaningful in biosensing applications. This all-in-fiber polymer Bragg grating exhibits high temperature sensitivity, excellent mechanical strength, and ultrahigh integration. As such, a temperature sensing element of this type would be a beneficial tool for biological measurements. © 2018 Optical Society of America

OCIS codes: (050.6875) Three-dimensional fabrication; (060.3735) Fiber Bragg gratings; (050.2230) Fabry-Perot; (060.2370) Fiber optics sensors.

https://doi.org/10.1364/OL.43.003409

Multiphoton polymerization (MPP) has become increasingly common for functional microdevice fabrication in recent years. Applications have included microfluidic devices, microelectromechanical systems, and metamaterials [1–3]. Microdevices fabricated using MPP exhibit several beneficial physical and chemical properties, such as high elasticity, nonlinearity, and thermal expansion coefficients [4,5]. Fiber Bragg gratings (FBGs) are a common fiber temperature sensor with an excellent linear temperature response, narrow bandwidth, and compact structure. However, silica FBGs are limited by a low thermo-optical coefficient ($\sim 6.45 \times 10^{-6}$/°C) and cannot achieve high temperature sensitivity (typically ∼10 pm/°C for commercial silica fibers) [6,7]. Polymer fiber Bragg gratings (PFBGs) are more advantageous for the high thermo-optical coefficient ($\sim -2 \times 10^{-4}$/°C) of the polymer material that composes the waveguide [8,9]. In 2011, Yuan *et al.* demonstrated FBGs developed from a TOPAS polymer optical fiber (POF), achieving a temperature sensitivity of −78 pm/°C [10]. In 2017, Marques *et al.* reported on a chirped FBG developed from a polymethyl methacrylate POF which achieved a temperature sensitivity of −131 pm/°C [11].

Establishing a reliable connection between the polymer waveguide (PW) and silica fiber is a critical issue restricting the development and use of PFBGs in fiber sensing systems. In this Letter, we seek to solve these connection problems by proposing an all-in-fiber PFBG fabricated with femtosecond (FS) laser micromachining [12]. The device is produced in four steps: splicing, ablation, polymerization, and washing. This PFBG solves connection problems and maintains sufficient mechanical strength. Its transmission spectrum was analyzed using a finite element method (FEM), and its temperature response was measured to be −220 pm/°C ranging from 24°C to 40°C, which is a significant improvement over previously reported FBGs in both the silica fiber and POF. The humidity response achieved is −36 pm/% relative humidity (RH) at 25°C range from 30% to 90% RH. In real application, the device has to be sealed in a section of glass tube to avoid the cross-sensitivity produced by humidity [13]. As such, the device could be beneficial for high-precision biological temperature measurements.

Figure 1 shows a schematic diagram of the PFBG microprinted using MPP in a silica tube (ST) spliced between two single-mode fibers (SMFs). A pair of polymer bases, designed to enhance cohesive strength, were included to make the overall structure more stable. A series polymer grating is used not only to generate Bragg resonance, but also to support the PW suspended in the air. During the printing of grating segments, the PW will be secondly irradiated by FS laser, resulting in the periodical refractive index (RI) modulation for Bragg resonance. Broadband light input from the lead-in fiber

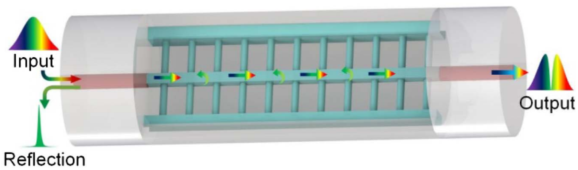

Fig. 1. Schematic diagram of the microprinted PFBG in a ST.

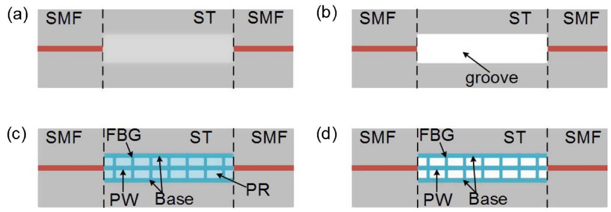

Fig. 2. (a) ST was spliced between two SMFs, and (b) a pair of grooves were drilled using a FS laser. (c) Polymer structure was then microprinted in the ST using MPP. (d) Any PR remaining in the ST was cleaned using an acetone and isopropyl alcohol mixture.

was transmitted to the lead-out fiber through a rectangular PW. The input light was modulated by the polymer grating, producing Bragg resonance in the spectrum. The microprinting technique can be divided into four steps.

Step 1: As shown in Fig. 2(a), an ST with a length of 800 μm and an internal/external diameter of 30/120 μm was spliced between two SMFs. If the splicing current is too high, the ST air hole will collapse. If the current is too low, the mechanical strength of the splicing point will be weak. Optimized splicing parameters for a multimode fiber included a splicing current of −10 bit for 400 ms (FUJIKURA 80 S fiber fusion splicer).

Step 2: As shown in Fig. 2(b), a pair of rectangular grooves with a size of 800 μm × 40 μm × 65 μm was used to open the ST air hole. They were drilled separately from the upper and lower ST surfaces using an FS laser. The sample was then carefully cleaned with alcohol under ultrasonic conditions to remove residual debris generated by FS laser ablation.

Step 3: As shown in Fig. 2(c), ST grooves were filled with a photosensitive resin (PR), resulting in a capillarity effect. The PR used in this experiment was a type of negative resin (Type: PP-1, purchased from Zhichu optics Co., Ltd., Shenzhen, China), which contains photo-initiator (IGR-369, Ciba-Geigy) and monomer (SR444, SR369, from Sartomer) compounds. The sample was then mounted on a 3D air-bearing stage (Aerotech) for structure polymerization. The utilized FS laser had a central wavelength of 1026 nm, a pulse width of 250 fs, and a repetition rate of 200 kHz. A pair of bases with dimensions of 800 μm × 10 μm × 11 μm was first polymerized along the inner ST surface to decrease the grating segment length and enhance cohesive strength between the ST and the polymerized structure. The PW and FBG segments were then polymerized by an oil objective with a numerical aperture of 1.4.

Step 4: As shown in Fig. 2(d), the sample was immersed in an acetone and isopropyl alcohol mixture (1:5) for 20 min, to wash away any remaining PR. After these four steps, the PFBG was successfully microprinted in the ST and integrated in an all-fiber system.

The light-guiding properties of this polymerized waveguide were experimentally investigated. First, the same laser, operating at a power of 1.94 mW with a scanning velocity of 200 μm/s, was employed to fabricate the PW and FBG. The FBG was polymerized using single scanning with a period of 1035 nm, and the PW was polymerized using snake scanning to increase its cross-sectional width. Figures 3(a)–3(c) show a series of scanning electron microscope (SEM) images for three samples with waveguide widths of 1810, 2360,

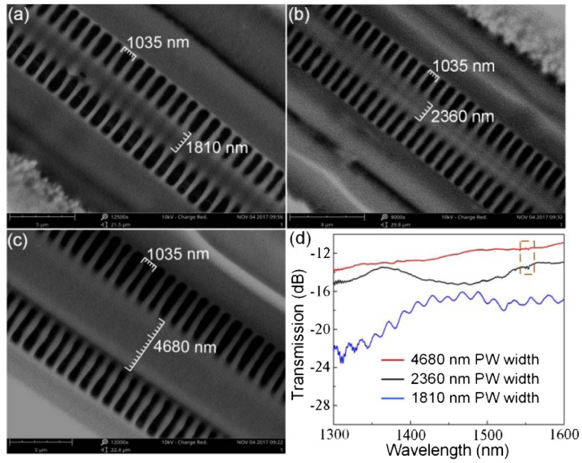

Fig. 3. SEM images of three PFBGs with waveguide widths of (a) 1810, (b) 2360, and (c) 4680 nm. The transmission spectra for the three PFBGs are shown in (d).

and 4680 nm before glass tube packing. The polymerized structure is evident in the figure. It is also clear that there is no adhesion, and the waveguide flatness has improved with increasing width. The transmission spectra of these three samples was measured using a broadband light source (1250–1650 nm) and an optical spectrum analyzer, the results of which are shown in Fig. 3(d). The insertion loss of this device decreased significantly (~6 dB at 1550 nm), as the width increased from 1810 to 4680 nm. This can be explained by improved modal radii matching between the PW and each SMF. Additionally, the apparent interference spectrum can only be observed at 1810 nm, which we believe is the result of multimode interference produced by a mode mismatch between the SMF and the PW [14].

As shown in Fig. 3(d), there is low Bragg reflection (~1557 nm) present in this spectrum because the same laser power was used to fabricate the PW and FBG. As such, the modulation intensity is not high enough to excite Bragg resonance [15,16]. The RI of the polymerized structures can be increased by increasing the FS laser power [17]. Therefore, to enhance the modulation intensity, differing laser powers of 1.94 and 1.30 mW were utilized at the same velocity (200 μm/s) to fabricate the FBG and PW. To obtain a stable PW with an apparent Bragg resonance, we have explored the optimal width of PW. When the PW width is similar to that of the SMF core, the Bragg resonance will be too weak to be observed. When the PW width is too small, its propagation loss will be significantly increased, and the multimode interference effect will become very significant. After a number of comparative experiments, we got the best PW width of ~4.68 μm. The resulting transmission and reflection spectrum of the polymerized FBG are shown in Fig. 4, where two transmission dips are observed at 1558.5 (1.2 dB) and 1554.0 nm (0.5 dB), and one reflection peak is observed at 1558.5 nm (16.5 dB). As a result, this can be classified as a few-mode type PW [18].

A Fabry–Perot (F-P) interferometer was constructed in the SMF to calibrate material dispersion of the polymer. A schematic diagram of this system is included in the inset image of Fig. 5. By the same method in Fig. 2, a PW with a length of 40 μm and a width of 10 μm was directly polymerized in a grooved SMF, which is drilled by an FS laser. The broadband

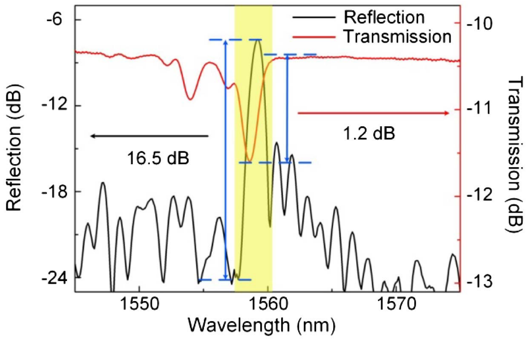

Fig. 4. Transmission and reflection spectrum for the PFBG.

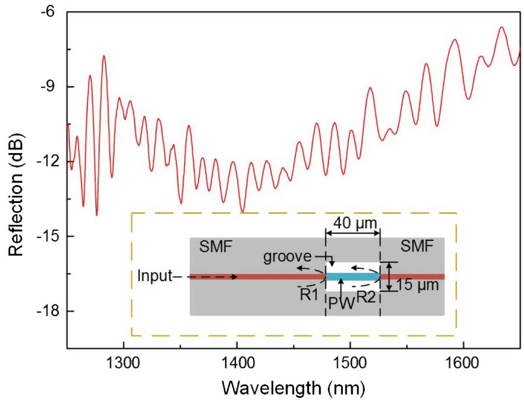

Fig. 5. Reflection spectrum for the PW-based F-P interferometer. The inset image shows a schematic diagram of this F-P interferometer.

light transmitted from the left SMF is reflected at the two interfaces (R1 and R2), and the resulting interference can be observed in the reflection. This process is shown in Fig. 5. The PW material RI can be calculated with Eq. (1) by measuring the free spectral range (FSR) of the F-P interference. This can be expressed as

$$\mathrm{FSR} = \frac{\lambda^2}{2nL}, \tag{1}$$

where λ is the wavelength, n is the RI of the PW material, and L is the length of the PW (40 μm). The RI of the PW material was calculated to be 1.543 (at 1507 nm), 1.538 (at 1528 nm), 1.531 (at 1558 nm), 1.523 (at 1588 nm), and 1.518 (at 1615 nm).

An FEM model was used to simulate modal properties for the PW, using its calculated RI and measured size (4.67 μm × 5.33 μm). Figure 6(a) shows the simulated relationship between the Bragg resonance wavelength and the grating period. It was calculated from Eq. (2):

$$m\lambda_b = 2n\Lambda, \tag{2}$$

where m is the order of the Bragg resonance, λ_b is the Bragg resonance wavelength, n is the effective RI, and Λ is the grating period. Figure 6(b) shows the measured transmission spectrum. The wavelengths of the two dips are in excellent agreement with simulated results and correspond to the LP01 (1558.5 nm) and LP11 modes (1554.0 nm). The small

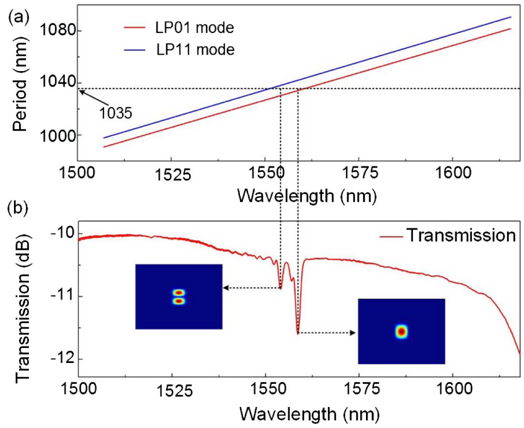

Fig. 6. (a) Simulated relationship between a Bragg resonance wavelength and grating period. (b) Measured transmission spectrum and simulated mode field (LP01 and LP11) for the two dips.

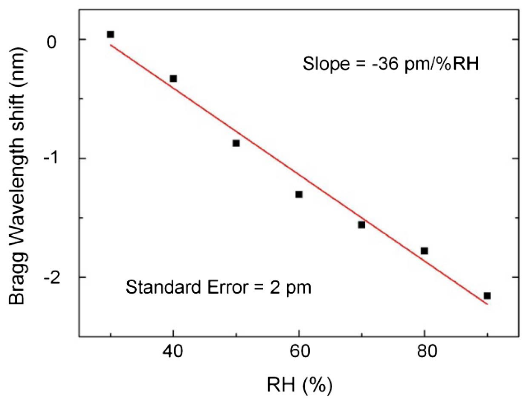

Fig. 7. Bragg wavelength shift evolution of the PFBG as the RH increased from 30% to 90%.

deviations may have resulted from errors in the measurement of PW dimensions.

The humidity response of the PFBG was measured using a controlled humidity chamber [19]. Before testing, the sample was placed in a drying oven for 24 h (at 20% RH and 21°C). The humidity measurement was done at 25°C, and the Bragg resonant dip (at 1558.5 nm) was used to monitor humidity change. The chamber was programmed to increase the RH from 30% to 90% with a step of 10% RH. The time between each RH step was 30 min, where 15 min was used to increase the RH, and 15 min was left for stabilization. The humidity sensitivity achieved is −36 pm/% RH with a standard error of 2 pm, as shown in Fig. 7. In real temperature measurements, the cross-sensitivity from humidity can be overcome by a glass tube package [20].

The temperature response of the PFBG was measured using a controllable furnace [21]. The Bragg resonant wavelength (~1558.5 nm) was used to monitor temperature changes during the experiment. The temperature was gradually increased from 24°C to 40°C with a step of 2°C and maintained for 15 min during each step (at 50% RH). Figure 8(a) demonstrates the spectral evolution of transmitted light, as the ambient temperature was increased. The blue shift in the Bragg

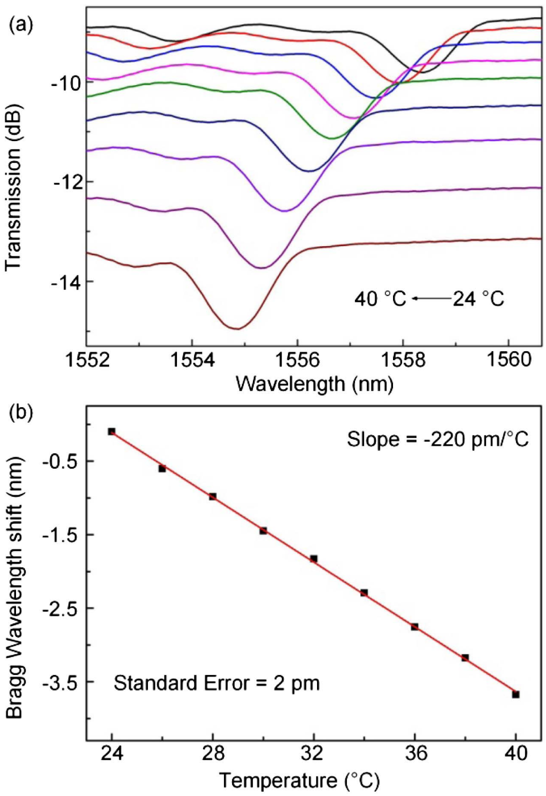

Fig. 8. (a) Spectral transmission evolution of the PFBG as the temperature increased from 24°C to 40°C. (b) Dip wavelength versus temperature.

resonant wavelength is clearly evident in this process. The attenuation of the sensor system is getting higher which can be the result of the reduced RI of polymer as temperature rises. Figure 8(b) illustrates the linear fitting of the Bragg resonant wavelength with temperature changes, achieving a sensitivity of −220 pm/°C with a standard error of 2 pm. This is 20 times higher than that of pure silica FBG and higher than previous reports on Bragg gratings in a POF [22]. The glass transition temperature (T_g) of the used resin is ∼100°C, which is demonstrated in the Sartomer product manual. Experimentally, the maximum operating temperature of this device is found to be 80°C. This enhanced temperature sensitivity can be explained by the high thermo-optical coefficient of the utilized polymer and completely suspended polymer structure.

In conclusion, we have demonstrated an all-in-fiber PFBG which was microprinted by an FS laser-induced MPP. This PFBG is composed of a base, a PW, and a FBG. The use of optimized laser power produces an obvious Bragg resonance in the transmission spectrum. A polymer F-P interferometer was fabricated in the SMF to calibrate PW material dispersion, and PW modal properties were simulated using FEM. These simulated results were in excellent agreement with the experiment and confirmed that the microprinted PW is a few-mode fiber with two transmission dips corresponding to the LP01 and LP11 modes. The RH response achieved is −36 pm/% RH. In real application, the cross-sensitivity produced by humidity can be solved by a glass tube package. Finally, a linear PFBG thermal response was achieved with a high sensitivity of −220 pm/°C. This FS laser-induced MPP could be a powerful new tool in the field of all-in-fiber devices and systems. This method is easy to be achieve and low in cost in real application.

Funding. National Natural Science Foundation of China (NSFC) (61575128, 61425007, 61635007); Natural Science Foundation of Guangdong Province (2015A030313541, 2015B010105007, 2014A030308007); Science and Technology Innovation Commission of Shenzhen (KQJSCX20170727101953680, JCYJ20160520163134575, JCYJ20160523113602609, JCYJ20160307143501276); Development and Reform Commission of Shenzhen Municipality Foundation.

REFERENCES

1. Y. L. Li, Y. F. Fang, J. Wang, L. Wang, and S. W. Tang, Lab Chip **16**, 4406 (2016).
2. D. Dendukuri, D. C. Pregibon, J. Collins, and T. A. Hatton, Nat. Mater. **5**, 365 (2006).
3. Y. F. Chen, J. R. Tao, and Z. Cui, Microelectron. Eng. **78-79**, 612 (2005).
4. H. Zou, S. S. Wu, and J. Shen, Chem. Rev. **108**, 3893 (2008).
5. J. A. Delaire and K. Nakatani, Chem. Rev. **100**, 1817 (2000).
6. M. Majumder, T. K. Gangopadhyay, A. K. Chakraborty, and K. Dasgupta, Sens. Actuators A **147**, 150 (2008).
7. D. Grobnic, S. J. Mihailov, J. Ballato, and P. D. Dragic, Optica **2**, 313 (2015).
8. C. Markos, A. Stefani, K. Nielsen, and H. K. Rasmussen, Opt. Express **21**, 4758 (2013).
9. G. Woyessa, A. Fasano, C. Markos, H. Rasmussen, and O. Bang, IEEE Photon. Technol. Lett. **29**, 575 (2017).
10. W. Yuan, L. Khan, and D. J. Webb, Opt. Express **19**, 1971 (2011).
11. C. A. F. Marques, P. Antunes, P. Mergo, and D. J. Webb, IEEE Photon. Technol. Lett. **29**, 500 (2017).
12. W. Xiong, Y. S. Zhou, X. N. He, Y. Gao, and M. Mahjouri-Samani, Light Sci. Appl. **1**, e6 (2012).
13. G. Woyessa, J. K. M. Pedersen, A. Fasano, K. Nielsen, C. Markos, and O. Bang, Opt. Lett. **42**, 1161 (2017).
14. P. F. Wang, G. Brambilla, M. Ding, Y. Semenova, Q. Wu, and G. Farrell, Opt. Lett. **36**, 2233 (2011).
15. K. K. Lee, A. Mariampillai, M. Haque, B. A. Standish, V. X. Yang, and P. R. Herman, Opt. Express **21**, 24076 (2013).
16. J. R. Grenier, L. A. Fernandes, and P. R. Herman, Opt. Express **21**, 4493 (2013).
17. T. Gissibl, S. Wanger, M. Schmid, and H. Giessen, Opt. Mater. Express **7**, 2293 (2017).
18. X. H. Feng, H. Y. Tam, and W. H. Chung, Opt. Commun. **263**, 295 (2006).
19. G. Woyessa, A. Fasano, C. Markos, and A. Stefani, Opt. Mater. Express **7**, 286 (2017).
20. Z. Y. Li, C. R. Liao, J. Song, Y. Wang, and F. Zhu, Photon. Res. **4**, 197 (2016).
21. Z. Zhang, C. R. Liao, J. Tang, Y. Wang, Z. Y. Bai, and Z. Y. Li, IEEE Photon. J. **9**, 7101109 (2017).
22. W. Yuan and A. Stefani, IEEE Photon. Technol. Lett. **24**, 401 (2012).